Dimer adsorption on square surfaces with first- and second-neighbor interactions

A.J. Phares [a,*], P.M. Pasinetti [b], D.W. Grumbine Jr. [c], F.J. Wunderlich [a]

[a] Department of Physics, Villanova University, Mendel Science Center, Villanova, PA 19085-1699, USA
[b] Departamento de Física, Instituto de Física Aplicada, Universidad Nacional de San Luis—CONICET, Chacabuco 910, 5700, San Luis, Argentina
[c] Department of Physics, Saint Vincent College, Latrobe, PA 15650-4580, USA

ABSTRACT

Dimer adsorption on surfaces simulates the adsorption of particles that bind onto two nearest-neighbor sites. In 1993, we constructed a transfer matrix (**T**-matrix) for the study of dimers on stepped surfaces, consisting of M-sites wide square terraces, considering only first-neighbor interaction energies. Here, we consider a more realistic model by including both first- and second-neighbor interaction energies, V and W. The non-trivial construction of the **T**-matrix to include second-neighbor interactions is used to obtain the low-temperature energy phase diagrams of the dimer system for any M, when first-neighbors are attractive, and for values of $M < 7$ when first-neighbors are repulsive. New crystallization patterns and phases are observed and extrapolated to infinite M. Monte Carlo simulation techniques confirm our **T**-matrix results, but the **T**-matrix method is found to be computationally more efficient and more precise. However, Monte Carlo parallel tempering simulations combined with finite-size scaling, while limited in precision, are more efficient to obtain the critical temperature of the various order–disorder transitions as a function of $W/|V|$, from the study of the heat capacity and the order parameter as functions of temperature. We also discuss the relevance of these results to experiments.

© 2011 Elsevier B.V. All rights reserved.

1. Introduction

The theoretical investigations of the dimer problem and dimer adsorption on surfaces with different geometries have been going on for several decades. Listing the achievements made over these decades goes well beyond the scope of this paper. There are a number of excellent review articles in the field and we would like to refer to one of the most recent ones by Wu [1]. Recently, by using Monte Carlo (MC) simulations, histogram reweighting, and finite-size scaling techniques, Rzysko et al. have studied a wide variety of systems in the presence of multisite occupancy [2–7]. Included among them are attracting dimers in the presence of energetic heterogeneity [2,3], heteronuclear dimers consisting of different segments A and B adsorbed on square lattices [4–6], and heteronuclear dimers in 3-dimensional systems [7]. In these leading papers, a rich variety of phase transitions was reported along with a detailed discussion about critical exponents and universality class.

The effect of second-neighbor interactions on the crystallization patterns of adsorbed dimers has not been investigated. The aim of this work is to study this effect when adsorption takes place on stepped surfaces consisting of M-sites wide, infinitely long (1 0 0) terraces, and on the infinite 2-dimensional (1 0 0) surface. There are two possible experimental applications. The first is that monomer particles, adsorbed onto two nearest-neighbor (first-neighbor) sites, often bond to form an adsorbed dimer. The other is that bridge adsorption of a particle between two first-neighbor sites often behaves as a dimer occupying these two sites. This is the case of, for example, CO-molecules with their C-ends bonding to two first-neighbor sites, when the substrate is Ni(1 0 0), Pt(1 1 1) [8], or Pd(1 1 1) [9].

The numerical computations on terraces of finite length L, and finite width M, are carried out using a transfer-like **T**-matrix method we have developed in 1993 [10]. Our method does not use periodic boundaries in the L or M direction, and yields a sparse **T**-matrix. All of the eigenvalues of this matrix contribute to the partition function Z of the system. For infinitely long terraces, we have shown that the only contribution to Z is its largest eigenvalue. Since this method does not use periodic boundaries and finite-size scaling, it is computationally much more efficient and precise than using Monte Carlo (MC) simulations to generate the low-temperature energy phase diagrams for infinitely long terraces. The extrapolation to infinite M (infinite 2-dimensional square surface) of the results obtained with the **T**-matrix method is possible and confirmed by MC simulations, which consider the extrapolation of the results on (1 0 0) surfaces having $L \times L$ atomic

* Corresponding author. Tel.: +1 610 519 4889; fax: +1 610 519 7465.
E-mail address: alain.phares@villanova.edu (A.J. Phares).

sites with the usual periodic boundary conditions in both the length and the width of the lattice. Sections 2–4 present our **T**-matrix method and its numerical application for finite M, and the extrapolation of its results in the infinite-M limit. Sections 5 and 6 are devoted to the results obtained in the infinite M limit using the more computationally efficient, but less accurate, MC simulations for the study of the order–disorder transitions. Section 7 discusses the experimental relevance of these theoretical findings.

Transfer matrix methods and MC simulation techniques are well-known and widely used. The **T**-matrix method we have developed for the study of dimers adsorbed on M-sites wide (1 0 0) terraces, limited to first-neighbor interactions, was first introduced in 1993, as mentioned above [10]. Several years later, we found this method capable of providing a unified treatment of monomer adsorption on terraces and nanotubes, not only for a number of different lattice geometries, but also for any number of pair-wise adsorbate–adsorbate interactions [11]. Dimer adsorption models, with non-periodic boundaries, are more difficult to develop beyond first-neighbor interactions. Unlike monomer adsorption, the construction of the **T**-matrix cannot be easily generalized to different lattice geometries, or for any number of pair-wise interactions. Even in the simplest case of a square geometry, the derivation that includes second-neighbor interactions is very lengthy as compared to the one presented in the 1993 paper, which considers only first-neighbor interactions. Without any derivation, Section 2 presents the elements necessary to recursively construct the **T**-matrix used in this study, in a manner that recovers the results of the 1993 paper as a special case. The MC simulation techniques, relevant to our investigation, are described in Section 5.

The notation used in this paper is the same as those used in recently published articles on monomer adsorption on surfaces, whether terraces or nanotubes, with equilateral triangular, or (1 1 1), geometry [12–19]. Here the stepped surface consists of infinitely long, M-sites wide, (1 0 0) terraces. A square cell represents a surface site, and a dumbbell, with its ends occupying the centers of two nearest-neighbor cells, represents an adsorbed dimer particle. The particles come from a medium, which is either a gas or a solution. Their chemical potential energy, μ', in the medium is determined by the pressure, if a gas, or the concentration, if a solution. The adsorbate–substrate interaction energy V_0 is assumed to be the same at step- and bulk-sites of the terraces, and the relevant quantity is the shifted chemical potential $\mu = \mu' + V_0$, from here on referred to as the chemical potential. First- and second-neighbor interaction energies between dimers are denoted V and W, with the convention that positive values refer to attraction and negative values to repulsion. The absolute temperature T of the system can be controlled and we assume thermodynamic equilibrium.

The medium-substrate system is characterized by three dimensionless parameters, $u = W/|V|$, $v = \mu/|V|$, and $t = kT/|V|$ (k is Boltzmanns constant), leading to a 3-dimensional temperature-energy phase space. The (uv)-plane is viewed as horizontal with the t-axis as vertical. Evolution of the system at constant temperature takes place in a horizontal section of the phase space. In this horizontal plane, when u is kept fixed while the reduced chemical potential (v) is varied, a crystallization pattern, or phase, is observed when the surface coverage remains unchanged over a relatively wide range of v. Thus, a series of phases, intermediate between zero-coverage (empty) and full coverage, are formed as the external pressure of the gas or concentration of the solution is increased, that is with increasing v. A numerical search in this (uv)-plane is conducted to obtain all of the possible phases that may appear at a given t. The largest number of intermediate phases occurs when the temperature is below a certain threshold

$t_0 = kT_0/|V|$, which varies with the width M of the terrace and the interaction energies. Using the **T**-matrix method, this threshold value is numerically found in the range 0.01–0.1 for the values of M considered. Experimentally, and for a typical value of $|V| = 15$ kcal/mol, this corresponds to a temperature T_0 in the range of 76–760 K. By setting $t < t_0$, one generates the low-temperature energy phase diagram. As t is increased, certain phases in the 2-dimensional (uv)-plane begin to disappear, and eventually one reaches a continuous transition from empty to full coverage with no intermediate phases.

Sections 3 and 4 present the numerical results, obtained using the **T**-matrix method, leading to the low-temperature energy phase diagrams for attractive and repulsive first-neighbors, with increasing terrace width M, and their extrapolation in the infinite-M limit. Sections 5 and 6 use MC simulations to obtain an estimate, from the heat capacity and the order parameter cumulant, of the critical temperature at which there is a transition from the ordered phases (determined in the infinite-M, or infinite-L, limit) to disorder, as a function of u.

2. The transfer matrix method

The technique of constructing the **T**-matrix for dimer adsorption on terraces or on nanotubes is very similar to that of monomer adsorption [11]. The major difference here is that the matrix is sparse. Following [11], the first step is to determine all possible occupational configurations of a row of M sites across the width of the square terrace, which provides the rank $D(M)$ of the **T**-matrix. This number is obtained recursively, as exemplified in Fig. 1. This figure considers the four possible states of occupation of the first atomic site on the right side of a row of M sites. The first state is a vacancy (0) indicated by a cross. The second state (1) is the one for which the other end of the dimer occupying this first site is in the row below; the third state (2) is the one for which the dimer's other end is in the row above; and the fourth state (3) is the one for which its other end is in the same row occupying the second site. Thus, in each of the first three cases, the number of all possible states of occupation is the number of states of the remaining $M-1$ sites, or $D(M-1)$. The number of states when the first two sites are occupied by a dimer is $D(M-2)$. Consequently,

$$D(M) = 3D(M-1) + D(M-2). \tag{1}$$

When $M=1$, there is only one site in the row, which may be in states (0), (1), or (2) yielding $D(1)=3$. Thus, the rank of the **T**-matrix is recursively obtained using Eq. (1) with the initial conditions $D(0)=1$ and $D(-1)=0$.

The ordering of all of the states of occupation of the M sites in a given row follows automatically from the recursive relation Eq. (1)
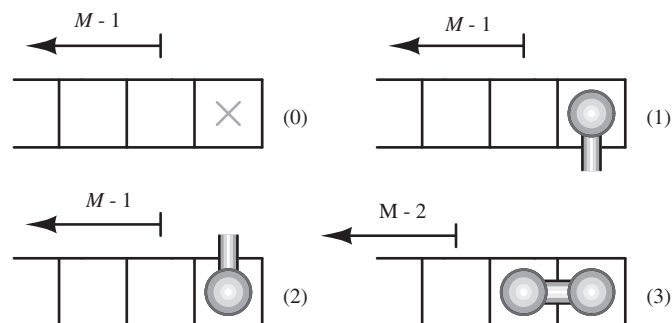

Fig. 1. The four possible states of occupancy of the first site in a horizontal row of M sites in the width of a square terrace. Only the first three sites are shown starting from the right side.

— first-neighbor interactions

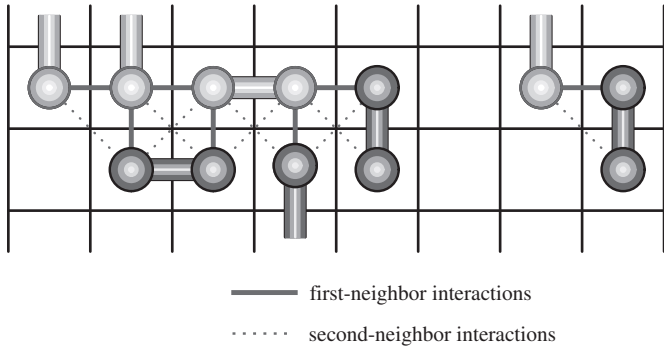······ second-neighbor interactions

Fig. 2. Two consecutive rows of $M=8$ sites in the width of a square terrace corresponding to a possible state of occupation by dimers. The states of dimer occupation of the top and bottom rows are associated with a given set column and row numbers of the **T**-matrix. The corresponding **T**-matrix element is then obtain as the product $x^a y^b z^c$, where a, b, and c are, respectively, given by the number of dimers indicated in light gray, the number of first-neighbors indicated in solid lines, and the number of second-neighbors indicated in dotted lines.

and the order chosen for the state of occupation of the first site. The ordered $D(M)$ configurational states are then used to label the row and column entries of the **T**-matrix. In this manner, a matrix element of row number i and of column number j corresponds to two specific configurational states, the i-state and j-state. The corresponding matrix element is obtained by considering *two consecutive rows* of M sites in the horizontal width of the lattice, such that the configurational state of occupation of the bottom row is the i-state and the occupational configuration of the top row is the j-state. When no matching between these two states is possible, the corresponding matrix element is zero. Non-zero elements are of the form $x^a y^b z^c$, where x, y, and z are the activities associated with μ, V, and W, namely,

$$x = \exp(\mu/kT), \quad y = \exp(V/kT), \quad z = \exp(W/kT). \quad (2)$$

Exponent a is the number of dimers in the top row of sites that do not have one end in the bottom row. Exponents b and c are, respectively, the numbers of first- and second-neighbors that occur between the dimers of the top row, and between the dimers of the top row and the dimers of the bottom row, following the selection rule exhibited in Fig. 2. In this figure, we show the state of occupation of two consecutive rows of a terrace 8-atoms wide. The top row is in the j-state and the bottom row in the i-state. The dimers considered to belong to the top row, indicated in light gray, are those that contribute to the number a. These dimers do not have an end belonging to the bottom row. In this case $a=4$. The remaining dimers, indicated in dark gray, belong to the bottom row. The first-neighbors that contribute to the number b (here $b=7$) are connected by solid lines. They occur between the ends of dimers located on the top row, and between the ends of dimers in the top row and those in the bottom row. The second-neighbors that contribute to the number c (here $c=8$), occurring between the ends of dimers found in the top row and those found in the bottom row, are connected by dotted lines.

The recursive construction of the **T**-matrix is based on the above analysis. The derivation is not straightforward but is very similar to the one derived in 1993 for dimers on a square lattice when only first-neighbor interactions are considered [10]. In this latter case, the **T**-matrix associated with dimer adsorption on an M-wide square terrace, $\mathbf{T}(M)$, is related to itself evaluated at $M-1$, and to four other matrices of different structures, **P**, **K**, **L**, and **J**, which are related to **T** and themselves evaluated at lower values of M. The notation used here to construct the **T**-matrix is chosen in such a way as to recover the results obtained in 1993 as a special case for which the second-neighbor interaction energy $W=0$, or $z=1$. There are two types of each of the **T**, **P**, or **K**

matrices, $\mathbf{T}_n$, $\mathbf{P}_n$, $\mathbf{K}_n$ ($n=1, 2$). For convenience, we label the **L**- and **J**-type matrices found in the absence of second-neighbor interactions as $\mathbf{L}_1$ and $\mathbf{L}_2$, respectively. In this manner, the reader can make the comparison between the relations obtained in the 1993-paper and the following relations:

$$\mathbf{T}_n(M) = \begin{bmatrix} \mathbf{T}_1(M-1) & 0 & xz^{n-1}\mathbf{P}_1(M-1) & xz^{n-1}\mathbf{K}_1(M-1) \\ \mathbf{T}_2(M-1) & 0 & xyz^{n-1}\mathbf{P}_2(M-1) & xyz^{n-1}\mathbf{K}_2(M-1) \\ 0 & z^{n-1}\mathbf{P}_2(M-1) & 0 & 0 \\ \mathbf{L}_1(M-1) & 0 & xyz^{n-1}\mathbf{L}_2(M-1) & xy^2z^{n+1}\mathbf{P}_2(M-2) \end{bmatrix}. \quad (3)$$

$$\mathbf{P}_n(M) = \begin{bmatrix} \mathbf{T}_1(M-1) & 0 & xyz^{n-1}\mathbf{P}_1(M-1) & xyz^{n-1}\mathbf{K}_1(M-1) \\ z\mathbf{T}_2(M-1) & 0 & xy^2z^n\mathbf{P}_2(M-1) & xy^2z^n\mathbf{K}_2(M-1) \\ 0 & yz^n\mathbf{P}_2(M-1) & 0 & 0 \\ z\mathbf{L}_1(M-1) & 0 & xy^2z^n\mathbf{L}_2(M-1) & xy^3z^{n+2}\mathbf{P}_2(M-2) \end{bmatrix}. \quad (4)$$

$$\mathbf{K}_n = \begin{bmatrix} z^{n-1}\mathbf{P}_1(M-1) \\ yz^n\mathbf{P}_2(M-1) \\ 0 \\ yz^n\mathbf{L}_2(M-1) \end{bmatrix}; \quad (5)$$

$$\mathbf{L}_n(M) = \begin{bmatrix} z^{n-1}\mathbf{T}_2(M-1) & 0 & xy^nz^n\mathbf{P}_2(M-1) & xy^nz^n\mathbf{K}_2(M-1) \end{bmatrix}. \quad (6)$$

The $\mathbf{T}_n(M)$ and $\mathbf{P}_n(M)$ are $D(M) \times D(M)$ matrices. The $\mathbf{K}_n(M)$ are $D(M) \times D(M-1)$ matrices, and the $\mathbf{L}_n(M)$ are $D(M-1) \times D(M)$ matrices. They satisfy the initial conditions $\mathbf{T}_n(0)=\mathbf{P}_n(0)=1$, and there are no $\mathbf{K}_n(0)$ or $\mathbf{L}_n(0)$. This completes the recursive construction of all of the matrices and $\mathbf{T}_1(M)$ is the **T**-matrix associated with dimer adsorption on an M-wide square terrace.

As follows from the general **T**-matrix formulation [11,10], the partition function $Z(M; x, y, z)$ associated with this adsorption study is obtained in terms of all of the eigenvalues of the transfer matrix $\mathbf{T}_1(M)$. However, in the limit as the length of the terrace becomes infinite, the largest eigenvalue $R(M; x, y, z)$, which is real and positive since all elements of $\mathbf{T}_1(M)$ are real and non-negative, is the only contribution to Z, namely,

$$Z(M; x, y, z) = R(M; x, y, z)^{1/M}. \quad (7)$$

At thermodynamic equilibrium, the statistical average of the coverage θ_0, the number per site of first-neighbors θ, and the number per site of second-neighbors β are

$$\theta_0 = \frac{2x}{MR}\frac{\partial R}{\partial x}, \quad \theta = \frac{y}{MR}\frac{\partial R}{\partial y}, \quad \beta = \frac{z}{MR}\frac{\partial R}{\partial z}. \quad (8)$$

The statistical average of the energy per site, ε, and the entropy per site divided by Boltzmann's constant, S (from here on referred to as entropy) follow as

$$\varepsilon = \mu\frac{\theta_0}{2} + V\theta + W\beta, \quad S = \frac{1}{M}\ln(R) - \frac{\varepsilon}{kT}. \quad (9)$$

The state of the adsorption system is then given by the set $\{\theta_0, \theta, \beta\}$ and the entropy S. The zero-coverage or empty phase $E = \{0,0,0\}$ with $S=0$ (perfect order) occurs at relatively low chemical potentials and the full coverage phase $F = \{1,(3M-2)/2M, 2(M-1)/M\}$ with $S \neq 0$ (partial order) occurs at relatively high chemical potentials. Kasteleyn has derived the values of S for semi-infinite square lattices of arbitrary width M, fully covered by dimers [20]. These values with increasing M are used as one of many checks of the validity of our numerical computations.

In the low-temperature energy phase diagram, consider two contiguous phases, $\{\theta_{01}, \theta_1, \beta_1\}$ and $\{\theta_{02}, \theta_2, \beta_2\}$, with differential values among their occupational characteristics, $\Delta\theta_0$, $\Delta\theta$, and $\Delta\beta$. It was shown in the past [11,10], that, when the transition between two phases is second-order, the point at which the

entropy has a local maximum occurs at the value of the chemical potential given by

$$v_t = -2(\Delta\beta/\Delta\theta_0)u - (\Delta\theta/\Delta\theta_0). \qquad (10)$$

It was also shown that, when the transition between two phases is first-order, the discontinuity occurs at the value of the chemical potential given by Eq. (10). This equation is used as a consistency check of the numerical results, and is used to report, in the low-temperature phase diagram, the equation of the boundary line between two phases. When the transition is second-order, the occupational characteristics θ and β, in the low temperature transition region, can be shown numerically to be linearly related to the coverage θ_0 according to

$$\theta = (\Delta\theta/\Delta\theta_0)(\theta_0 - \theta_{01}) + \theta_1, \quad \beta = (\Delta\beta/\Delta\theta_0)(\theta_0 - \theta_{01}) + \beta_1, \qquad (11)$$

3. Low-temperature energy phase diagram: attractive first-neighbors

The low-temperature energy phase diagrams for attractive first-neighbors ($V > 0$) were determined for terraces width M up to and including $M=8$. All of the numerical results are found to fit exact analytic expressions in M and are grouped into even and odd M series.

For M even, the phase diagram has two u-regions, $u < -1/2$ and $u > -1/2$. In the first region, the phases intermediate between empty (E) and full (F) coverage are $\{1/2, 1/4, 0\}$, which is perfectly ordered, and $\{(M+2)/2M, (M+6)/4M, 2/M\}$, which is partially ordered. The entropy of the latter phase is numerically obtained in terms of the golden ratio $\varphi = (1+\sqrt{5})/2$, namely $S = (1/M)\ln\varphi$. In the second u-region, $u > -1/2$, there are no intermediate phases, as shown in Figs. 3 and 4. The transitions between phases are all first-order. However, at the discontinuity between E and $\{1/2, 1/4, 0\}$, which occurs at $v = -1$, the numerical results show an equal mixture of patches of vacant sites and of patches of the perfectly ordered $\{1/2, 1/4, 0\}$ phase.

For M odd, the phase diagram has the same two u-regions, as shown in Fig. 4. The difference occurs in the first region, $u < -1/2$, where there is only one phase between E and F, namely, $\{(M+1)/2M, (M+1)/4M, 0\}$, which is perfectly ordered. Again, the transition between phases are all first-order; and at the
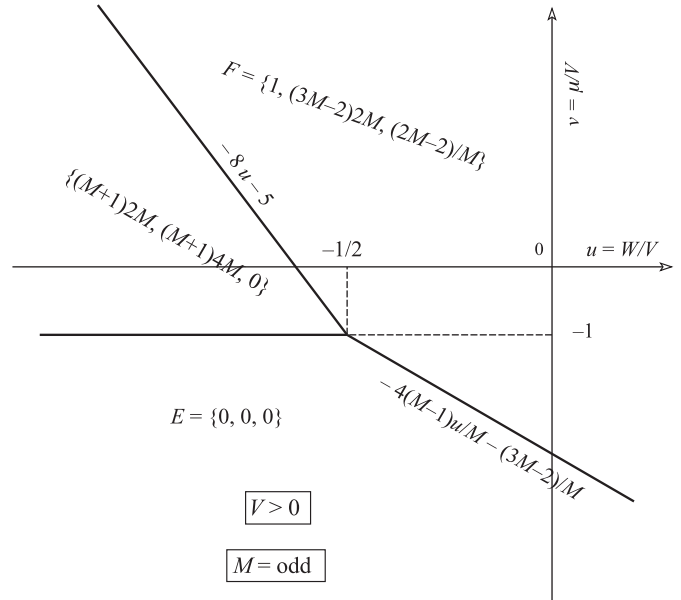

Fig. 4. Low-temperature energy phase diagrams for terraces M sites wide (M odd) in the case of attractive first-neighbors, $V > 0$.

discontinuity between E and $\{(M+1)/2M, (M+1)/4M, 0\}$, which occurs at $v = -1$, the results show an equal mixture of patches of vacant sites and of patches of the ordered phase $\{(M+1)/2M, (M+1)/4M, 0\}$. As expected, the two series of phase diagrams have the same infinite-M limit.

4. Low-temperature energy phase diagram: repulsive first-neighbors

For repulsive first-neighbors ($V < 0$), the low-temperature phase diagrams with increasing M do not show the similarities obtained in the attractive case. The individual phase diagrams can show the gradual progression toward the infinite-M limit. Most importantly, they can be used as a guide in suggesting new experiments on dimer adsorption on (1 0 0) stepped surfaces, and in analyzing the newly acquired data to determine the interaction energies from the observed phases. Table 1 provides the characteristics of all of the phases that could be observed at low temperatures for values of M up to and including $M=7$. The low-temperature energy phase diagram for a given M is unique, and could, in principle, be generated from the list of phases in Table 1. The phase diagram for $M=7$, given in Figs. 5 and 6, is presented as a sample. To conserve space, the other diagrams are available upon request. Excluding empty and full coverage, the occupational configurations of a number of non-trivial phases, which show common patterns with increasing M, are grouped into series in M. These are:

1. The series $\{(M+1)/3M, 0, 0\}$ is partially ordered. Phase $\{8/21, 0, 0\}$ belongs to this series and appears in the phase diagram of Figs. 5 and 6, which corresponds to $M=7$. This series consists of a mixture of horizontal and vertical dimers with no first- or second-neighbors. The entropy (per site) changes with M following two subseries, one for even and the other for odd M. For even M up to and including $M=8$, the numerical results give $S = (1/6M)\ln(M/2)$, which can be derived theoretically, and shows that it approaches zero in the infinite-M limit. We were unable to find closed form expressions for the numerical values of S obtained for odd M. These values are listed in Table 1.
2. The series $\{1/2, (M-2)/4M, 0\}$, valid for even M, and $\{(M+1)/2M, (M+1)/4M, 0\}$, valid for odd M are perfectly ordered,
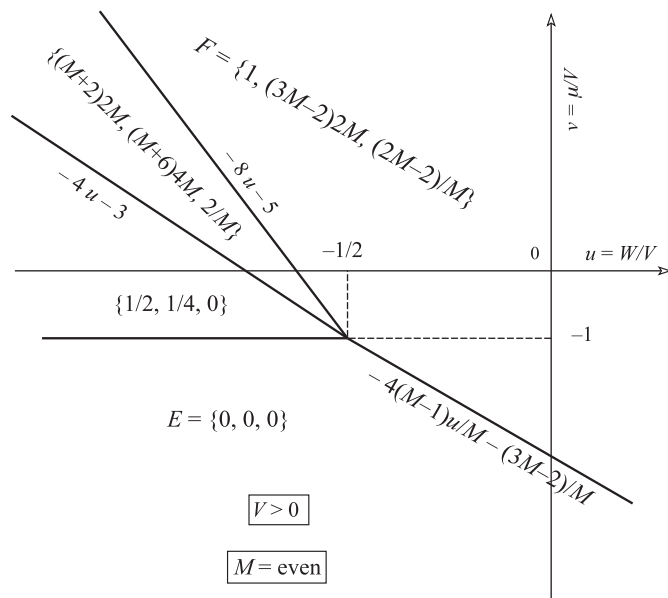

Fig. 3. Low-temperature energy phase diagrams for terraces M sites wide (M even) in the case of attractive first-neighbors, $V > 0$.

Table 1
Occupational characteristics of all of the phases, encountered at low temperature, of dimer adsorption on square terraces with $M=2$ to 7-sites wide.

| M	θ_0	θ	β	S
2	1/2	0	0	0
	1/2	0	1/4	0
	2/3	1/6	1/2	0
	3/4	3/8	1/2	1/8 ln 2
3	4/9	0	0	0
	1/2	0	1/6	0
	1/2	0	1/3	0
	2/3	1/3	0	0
	2/3	2/9	4/9	1/9 ln 2
	2/3	2/9	2/3	0
	4/5	8/15	8/15	1/15 ln 2
	4/5	8/15	4/5	1/15 ln 2
	6/7	2/3	16/21	1/21 ln 2
4	5/12	0	0	1/24 ln 2
	1/2	0	1/4	0
	1/2	0	3/8	0
	1/2	1/8	0	0
	2/3	1/4	7/12	1/12 ln 2
	2/3	1/4	3/4	0
	3/4	7/16	11/16	0
	3/4	7/16	11/16	0
	3/4	1/2	1/2	0
	4/5	11/20	17/20	0
	7/8	13/16	1	0.163624
5	2/5	0	0	0.056239
	12/25	0	6/25	0
	1/2	0	2/5	0
	8/15	1/15	1/3	0
	14/25	3/25	8/25	0
	3/5	3/20	1/2	0
	3/5	3/20	3/5	0
	3/5	3/10	0	0
	2/3	4/15	8/15	0
	2/3	4/15	4/5	0
	4/5	3/5	4/5	0
	4/5	3/5	24/25	0.064377
6	7/18	0	0	1/36 ln 3
	1/2	0	1/3	0
	1/2	0	5/12	0
	1/2	1/6	0	0
	7/12	1/8	1/12	0
	3/5	7/45	19/30	0
	2/3	5/18	11/18	0
	2/3	5/18	5/6	0
	2/3	5/12	1/3	0
	7/10	23/60	19/30	0.038508
	11/15	31/60	3/5	0.049928
	3/4	23/48	11/12	1/24 ln 2
	25/33	17/33	53/66	0.037657
	23/30	31/60	9/10	1/30 ln 3
	23/30	11/20	4/5	0
	23/30	17/30	23/30	1/30 ln 2
	7/9	5/9	8/9	0
	4/5	19/30	31/30	0
	5/6	3/4	1	0.126471
	5/6	11/12	4/3	0
7	8/21	0	0	0.051076
	10/21	0	2/7	0
	1/2	0	3/7	0
	11/21	1/21	8/21	0
	4/7	2/7	0	0
	4/7	3/28	1/2	0
	38/63	1/6	2/3	0
	13/21	11/42	8/21	1/42 ln 2
	2/3	2/7	2/3	0
	2/3	2/7	6/7	0
	36/49	23/49	38/49	0
	3/4	27/56	13/14	0
	58/77	38/77	10/11	0
	16/21	11/21	8/9	0
	27/35	41/70	4/5	2/35 ln 2
	60/77	45/77	68/77	0
	39/49	63/98	44/49	2/49 ln 2
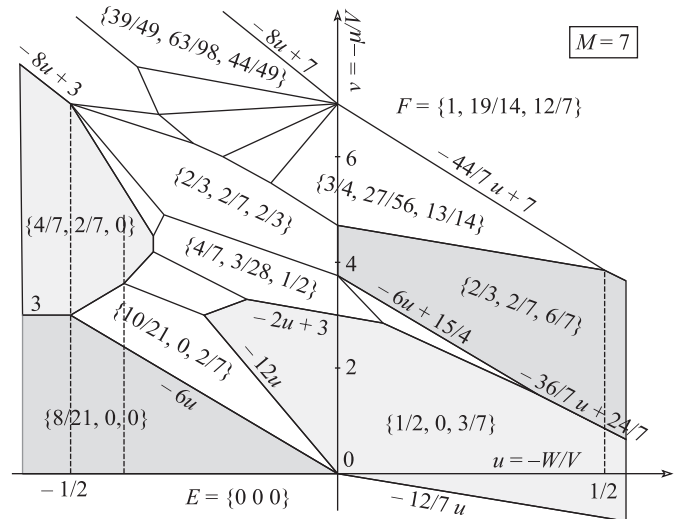
Fig. 5. Low-temperature energy phase diagram for a terrace $M=7$ sites wide in the case of repulsive first-neighbors, $V<0$ (for $u<1/2$).
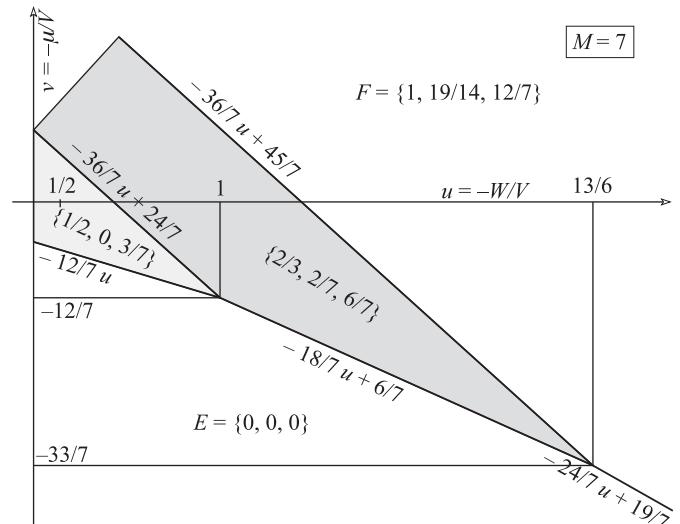

Fig. 6. Low-temperature energy phase diagram for a terrace $M=7$ sites wide in the case of repulsive first-neighbors, $V<0$ (for $u>1/2$).

and correspond to dimers parallel to the edges of the terrace. In the infinite-M limit, they all merge to the {1/2, 1/4, 0} phase which is also found for attractive first-neighbors. Phase {4/7, 2/7, 0} of Fig. 5 belongs to the series valid for odd M, since $M=7$ in that case.

3. There is another 1/2-coverage series of perfectly ordered phases, {1/2, 0, $(M-1)/2M$}, valid for both even and odd values of M, which corresponds to {1/2, 0, 3/7} for $M=7$ and appears in the phase diagram of Figs. 5 and 6. There exists only one occupational configuration of dimers with these occupational characteristics, for which all dimers are parallel to the edges of the terrace. Here the transition from empty to {1/2, 0, $(M-1)/2M$} is first-order for all M.

4. Finally, there is a 2/3-coverage series, {2/3, $(M-1)/3M$, $(M-1)/M$}, valid for both even and odd values of M, which has a zero-entropy per site, and corresponds to dimers that are parallel to the edges of the terrace. For $M=7$, this corresponds to the phase {2/3, 2/7, 6/7}, which appears in Figs. 5 and 6. In this series of phases, there are 2^{M-1} zigzag occupational configurations of dimers that can only be parallel to the edges of the terrace while satisfying the required occupational characteristics. The entropy

per site (divided by Boltzmann's constant) is the natural logarithm of the number of occupational configurations, $\ln 2^{M-1}$, divided by the number of sites, which is infinite for an infinitely long terrace. It is numerically verified that the entropy per site is exactly zero for all M. Therefore, the infinite-M limit of this series of phases, {2/3, 1/3, 1}, has zero-entropy per site, and an infinite number of zigzag occupational configurations of parallel dimers. There are energy regions with boundaries that are M-dependent with a direct transition from empty to this phase, and from this phase to full coverage. Both transitions are first-order for all M.

For any finite value of M, there is no common boundary between the phase, {1/2,(M−2)/4M,0} for even M, or {(M+1)/2M, (M+1)/4M,0} for odd M, and the phase {1/2,0,(M−1)/2M}. The remaining possible transitions between the above series of phases are second-order, and are listed in Table 2 as, transition (a), E→ {(M+1)/3M,0,0}, transition (b), from {(M+1)/3M,0,0}→{1/2, (M−2)/4M,0} for even M, or {(M+1)/2M,(M+1)/4M,0} for odd M, and transition (c), {1/2,(M−2)/4M,0}→{2/3,(M−1)/3M, (M−1)/ M}. In Table 2, we provide the maximum entropy and the corresponding coverage. The reduced chemical potential at which this occurs, and the corresponding values of first- and second-neighbors per site, are numerically verified as given by Eqs. (10) and (11), and consequently are not reported.

The phases identified in Table 1 that do not belong to any of the above series have configurational occupations in the bulk of the terrace that are similar to the features found in these series. The crucial question is whether the series of phases identified above are the only ones that survive in the infinite-M limit. This could not be answered in an unequivocal way. A number of the phases listed in Table 1 showed occupational configurations that were very similar to those of the identified series, while others did not show any particular pattern. The answer is given by MC simulations and finite-size scaling computations, described in Section 5. These computations show in a definite manner that, for the infinite two-dimensional (2-D) surface, there are no non-trivial phases other than those obtained by extrapolation of the series identified above, namely, {1/3, 0, 0}, {1/2, 1/4, 0}, {1/2, 0, 1/2} and {2/3, 1/3, 1}. The low-temperature energy phase diagram for dimer adsorption on the 2-D surface follows as shown in Fig. 7.

Section 6 is the study of the order–disorder transition from any of the four ordered phases of the 2-D surface as the temperature of the system is increased.

5. The Monte Carlo simulation method

Monte Carlo (MC) simulations in the canonical ensemble are applied to study the critical behavior of the system using finite-size scaling technique as L is increased to the point where edge effects become negligible. The focus is on the determination of the critical temperature, t_c, of the order–disorder transition and its

dependence on the parameter u. The simulations are carried out as follows:

- The lattice sites are arranged in a square structure of size $L \times L$, with conventional periodic boundary conditions in both directions.
- Appropriate values of L are used in such a way that the adsorption structures at the critical regime are not perturbed.
- The analysis is conducted for repulsive first-neighbors, because in the attractive case and at low temperature, the only non-trivial phase in the infinite-L limit is {1/2, 1/4, 0}, which is also observed in the repulsive case.
- Both repulsive and attractive second-neighbor interactions are considered.

We have used an efficient exchange MC or simulated tempering method [21,22]. As in Ref. [21], we build a compound system that consists of m non-interacting replicas of the system concerned, which are copies of the complete system: the $L \times L$ sites with their own occupational states, $\mathbf{X}_i$, where $i=1\ldots m$. The ith replica is associated with a heat bath at temperature t_i (or $\beta_i = 1/t_i$). This method of simulating several temperatures in a single run has a faster convergence and is much less time demanding than performing independent simulations each at a single temperature.

To determine the set of temperatures t_i, the highest temperature t_1 is chosen to be in the range of the disordered phase, where the relaxation (correlation) time, τ, is expected to be very short, and there is only one minimum in the free energy space. The
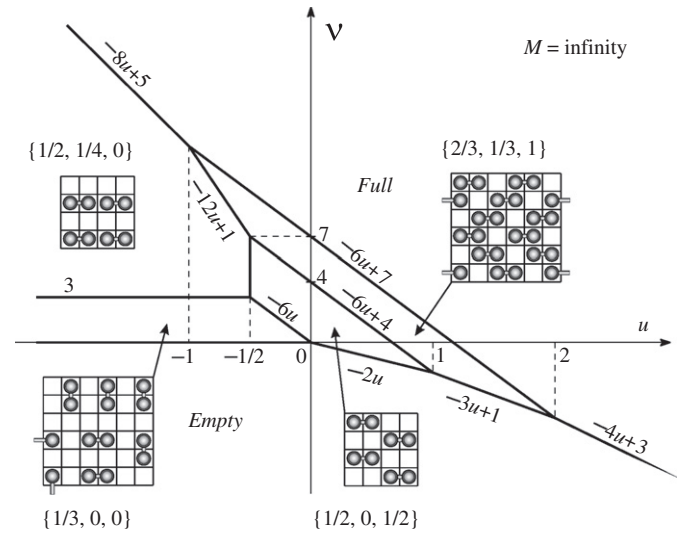

Fig. 7. The low-temperature energy phase diagram in the infinite-width limit of a terrace in the case of repulsive first-neighbors.

Table 2
Low temperature occupational characteristics at transition (a) between empty and the {(M+1)/3M,0,0} phase; at transition (b) between the {(M+1)/3M,0,0} phase and, either {1/2,(M−2)/4M,0} valid for even M, or {(M+1)/2M,(M+1)/4M,0} valid for M odd; and at transition (c) between {1/2,(M−2)/4M,0} and {2/3,(M−1)/3M,(M−1)/M}.

M	Transition (a)		Transition (b)		Transition (c)	
	θ_0	S	θ_0	S	θ_0	S
2	2/7	(1/2) ln 2	N/A	N/A	0.588504411	0.140599787
3	0.251559621	0.317295223	0.548660785	0.187466383	0.593866863	0.123489979
4	0.245815066	0.312611447	0.453411112	0.101916235	0.597022973	0.115817416
5	0.236489921	0.307485654	0.493198860	0.168974512	0.598978417	0.111565430
6	0.231297196	0.303758725	0.439574480	0.125600041	0.600271977	0.108888704
7	0.228139809	0.301586857	0.469107941	0.161148002	0.601179603	0.107055819

lowest temperature t_m is chosen in the range of one of the ordered phases being investigated. Finally, the difference between any two consecutive temperatures, t_i and t_{i+1} with $t_i > t_{i+1}$, is set at $t_i - t_{i+1} = (t_1 - t_m)/(m-1)$.

Under these conditions, the algorithm to carry out the simulation process is built on the basis of two subroutines:

(i) *Replica update*: Interchange vacancy-dimer. The procedure is as follows. (a) One out of the m replicas is randomly selected, for example, the ith replica, and is identified by its temperature t_i. (b) A dimer and a vacancy, both belonging to the replica chosen in (a), are randomly selected and their coordinates are established. (c) An attempt is made to interchange its occupancy state with probability $G = \min[1, \exp(-\Delta h)]$, as given by the Metropolis rule [23], where $\Delta h = \Delta H/kT$ represents, at temperature T, the dimensionless change in the energy of the system due to the interchange between a dimer and two vacant adjacent sites (vacancy).

(ii) *Exchange.* Exchange of the two configurations (occupational states) $\mathbf{X}_i$ and $\mathbf{X}_j$, corresponding to the ith and jth replicas, respectively, is tried and accepted with probability $G(\mathbf{X}_i, \beta_i | \mathbf{X}_j, \beta_j)$. In general, the probability of exchanging configurations of the ith and jth replicas is given by [21]

$$G(\mathbf{X}_i, \beta_i | \mathbf{X}_j, \beta_j) = \begin{cases} 1 & \text{for } \Delta \leq 0 \\ \exp(-\Delta) & \text{for } \Delta > 0 \end{cases}, \qquad (12)$$

where $\Delta = (\beta_i - \beta_j)[h(\mathbf{X}_j) - h(\mathbf{X}_i)]$. As in Ref. [21], we restrict the replica exchange to the case $j = i+1$, since for non-adjacent replicas that probability is negligible.

The complete simulation procedure consists of four steps: (1) initialization, (2) replica update, (3) exchange, and (4) repeat from step (2), $m \times L \times L$ times. This simulation process is referred to as a Monte Carlo step (MCs). The initialization of the compound system of m replicas, step (1), is as follows. One fixes the coverage θ_0 and the $N (= \theta_0 L^2)$ dimers are randomly distributed. The configuration of replica 1 is obtained after n_1 MCs' at temperature t_1 (MCs' consists of $L \times L$ realizations of the replica update subroutine). Second, for $i = \{2, \ldots, m\}$, the configuration of the ith replica is obtained after n_1 MCs' at t_i, taking as the initial condition the configuration of the replica to t_{i-1}. This method results in a more efficient than a random initialization of each replica.

Steps (1)–(4) are repeated for increasing lattice sizes as required by finite-size scaling. For each lattice, the equilibrium state can be well-reproduced after discarding the first n_2 MCs. Then, averages are taken over n_{MCs} successive MCs. Successive test simulations are carried out by doubling, each time, numbers n_1, n_2, and n_{MCs} and by observing the changes in the different observables until the fluctuation level drops below 5 percent. Values of $n_1 = 10^5$ and $n_2 = n_{\text{MCs}} = 5 \times 10^5$ were found to be sufficient in almost all cases. In the particular case of $\theta_0 = 2/3$ in the region $u < 0$, and also in some low-temperature cases, up to 10^6 MCs were necessary. Comparatively, it would be necessary for roughly ten times more MCs in the case of applying the standard MC algorithm, without the replica exchange mechanism, to obtain similar results.

As mentioned above, a set of equally spaced temperatures is chosen in order to accurately calculate the physical observables in the close vicinity of t_c. The thermal average $\langle Q \rangle$ of a physical quantity Q is obtained through simple averages,

$$\langle Q \rangle = \frac{1}{n_{\text{MCs}}} \sum_{\tau=1}^{n_{\text{MCS}}} Q[\mathbf{X}_i(\tau)]. \qquad (13)$$

Here $\mathbf{X}_i$ stands for the state of the ith replica (at temperature t_i) and τ stands for the simulation time or MC steps.

The heat capacity at constant volume C (in units of k) is sampled from energy fluctuations,

$$C(T) = \frac{C_L}{k} = \frac{\langle h^2 \rangle_T - \langle h \rangle^2}{L^2}, \qquad (14)$$

where h represents the dimensionless energy and L^2 the volume of the system. In most of the cases, the value of t at which the maximum of C occurs, for the largest value of L considered, is a good estimate of the critical temperature of the order–disorder transition.

As is standard for order–disorder phase transitions, an *order parameter* φ is introduced. The resulting adsorption structures shown in Fig. 7 present a strong orientational symmetry of the dimers, both for $\theta_0 = 1/2$ and $2/3$. These configurations allow the definition of an order parameter based on the orientation instead of considering partial coverages of different sublattices. Thus, a possible definition of φ is

$$\varphi = \frac{|N_v - N_h|}{N}, \qquad (15)$$

where N_v and N_h represent the numbers of vertical and horizontal dimers, respectively, and $N = N_v + N_h = \theta_0 L^2$. This order parameter has a minimum when both orientations appear in equal numbers and the system is disordered, which occurs at $t > t_c$. A preferred orientation, or ordered phase, appears when the temperature drops below the critical value t_c, where φ reaches a maximum. This choice of order parameter has been shown in previous works [24,25] to be more efficient in the study of the order–disorder phase transitions than the one obtained from sublattice coverages.

The reduced fourth-order cumulant, $U_L(T)$, for a given size L, introduced by Binder [26] is related to the order parameter according to

$$U(T) = 1 - \frac{\langle \varphi^4 \rangle_T}{3 \langle \varphi^2 \rangle_T^2}. \qquad (16)$$

Another way to estimate the critical temperature is from the temperature dependence of $U(T)$, as follows from finite-size scaling theory. This theory indicates that $U(T_c)$ is independent of L. In other words, the scaled critical temperature, t_c, is determined from the intersection of the curves $U(T)$ for various values of L.

Finally, in order to discuss the nature of the transition, we calculate the fourth-order energy cumulant U_E, which is defined in a manner similar to that of the Binder cumulant, U, of Eq. (16)

$$U_E(T) = 1 - \frac{\langle h^4 \rangle_T}{3 \langle h^2 \rangle_T^2}. \qquad (17)$$

6. Results from the Monte Carlo simulations

As described in Section 5, two methods are used to determine the critical temperature t_c of the order–disorder transitions. One relies on the properties of the fourth-order cumulant of the order parameter, and the other determines t_c from the location of the maximum of the heat capacity C. The efficiency and applicability of each method depend on the phase under study and the u-region in which it is found in the low-temperature phase diagram.

The dependence on u of the critical temperature, t_c, of the order–disorder transition for the 1/2-coverage phase found in the region $-1/2 < u < 1$, or $\{1/2, 0, 1/2\}$, is shown in Fig. 8. In this case, the position of the heat capacity maximum for the largest system ($L = 96$) provides an estimate of t_c. The t_c versus u curve reaches a maximum at approximately $u = 0.2$. As u is varied from repulsive to attractive second-neighbors, the data shows no discontinuity at $u = 0$, corresponding to no second-neighbor
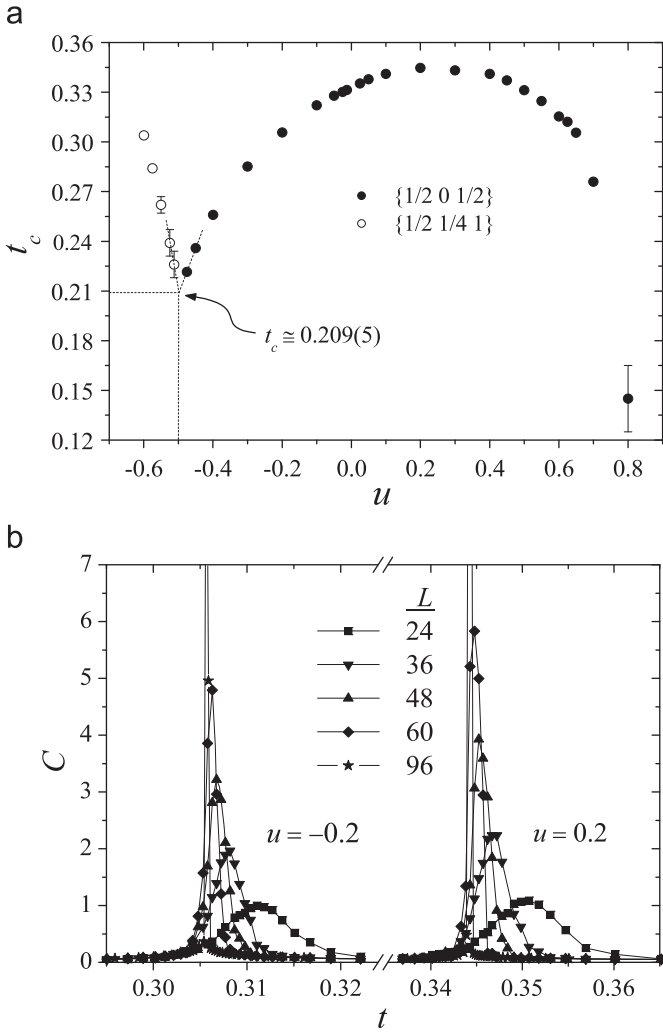
a

b

Fig. 8. (a) Critical temperature t_c versus u ($= W/|V|$) at 1/2-coverage, corresponding to the phase {1/2, 0, 1/2}, found in the energy range $-1/2 < u < 1$. The error estimate for each point is smaller than the size of the symbol used to represent it. The data were obtained by extrapolation of the maximum of the heat capacity to the infinite size L of the lattice. (b) Extrapolation of the maximum of the heat capacity to the infinite size L of the lattice for the points at $u = -0.2$ and 0.2.
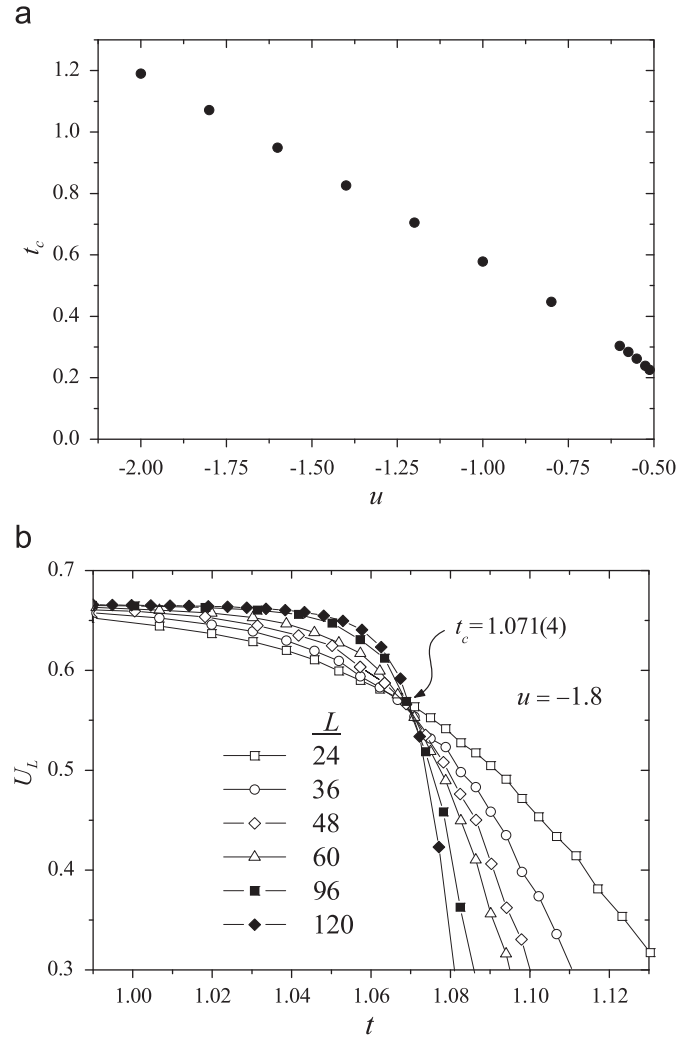
a

b

Fig. 9. (a) Same as Fig. 8(a) applied to the phase {1/2, 1/4, 0} found in the energy region $u < -1/2$. (b) The critical temperature t_c is obtained from the intercept of all of the curves, for different sizes L, of the order parameter cumulant, U, versus t for the value $u = -1.8$. The error in each measurement is smaller than the size of the symbols.

interactions. At this point, the critical temperature is $t_c \cong 0.332$; this is in agreement with the computations previously obtained in Refs. [24,27] for the case of dimers ($k = 2$) where second-neighbor interactions were not considered.

The other 1/2-coverage phase, {1/2, 1/4, 0}, occurs in the region $u < -1/2$. In this case, the u-dependence of t_c was obtained from the cumulant-crossing method, as is shown in Fig. 9, for system sizes up to $L = 120$. The tail end of this curve, as it approaches $u = -1/2$, is also shown on the t_c-plot that corresponds to the other 1/2-coverage phase in Fig. 8. In this plot, the two curves on either side of $u = -1/2$ clearly show a cusp formation at the boundary, which is obtained by linear extrapolation as $t_c \cong 0.209(5)$.

The 2/3-coverage phase, {2/3, 1/3, 1}, occurs in the region $-1 < u < 2$. The t_c-curve shown in Fig. 10 has been obtained also from the cumulant-crossing method, for sizes $L = 96$, 120, 180, and 240. The t_c-curve presents a monotonic behavior that drops to almost zero as u approaches $-1/2$ (in the region $-1 < u < -1/2$, the critical temperature is so low that it could not be numerically computed). The curve has no discontinuity at $u = 0$ (no second-neighbor interactions) where it takes the value $t_c \cong 0.18$, in agreement with previous results obtained in Ref. [25] where second-neighbor interactions were not considered.

For the 1/3-coverage phase, {1/3, 0, 0}, which occurs in the region $u < 0$, we considered lattice sizes up to 96×96. This phase is highly degenerate and the critical temperature is very low. This is why it is very difficult to perform accurate simulations with increasing values of L, and ultimately reach the level of confidence previously obtained in the finite-size scaling limit. The order-disorder transition for this phase is determined from the heat capacity curves for $L = 96$. These curves have a very broad maximum resulting in large error bars in the determination of t_c, as shown in Fig. 11. Despite the qualitative character of these results, it is still possible to observe a very clear increasing trend with increasing values of $|u|$.

Finally, to determine the order of the phase transitions, we use finite-size analysis of the energy cumulant, U_E, and of the order parameter cumulant, U, as functions of t, while one increases the lattice size, L. The U_E-curves have a minimum, which is expected to become sharper and deeper as L increases, when the transition is first-order [26]. Otherwise the minimum of the U_E-curves levels off and approaches the value of 2/3, as expected for a continuous or second-order phase transition. On the other hand, the U-curves develop a sharp negative minimum with increasing L, when the transition is first-order; otherwise the U-curves smoothly drop from 2/3 to 0, for a continuous or second-order transition [28–31]. Samples of these results are shown in Fig. 12(a–c).
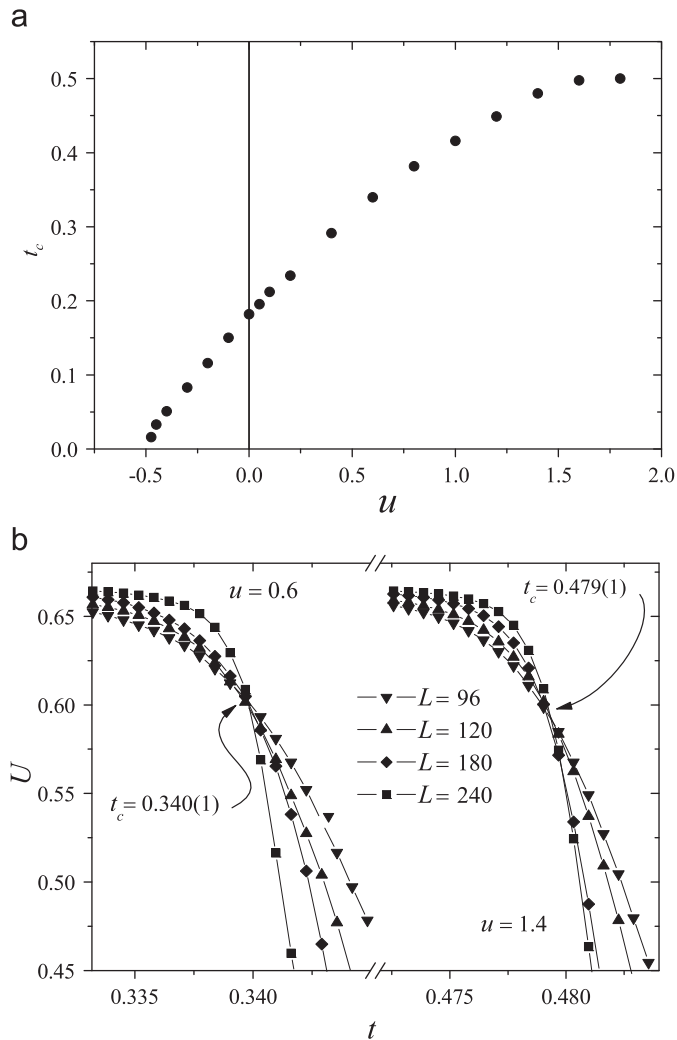
a

b

Fig. 10. (a) Same as Figs. 8(a) and 9(a) applied to the phase {2/3, 1/3, 1} found in the energy region $-1 < u < 2$. (b) The critical temperature t_c is obtained by extrapolation of the maximum of the heat capacity to the infinite lattice size L, for $u = 0.6$ and 1.4. The error in each measurement is of the order of the symbol's size.
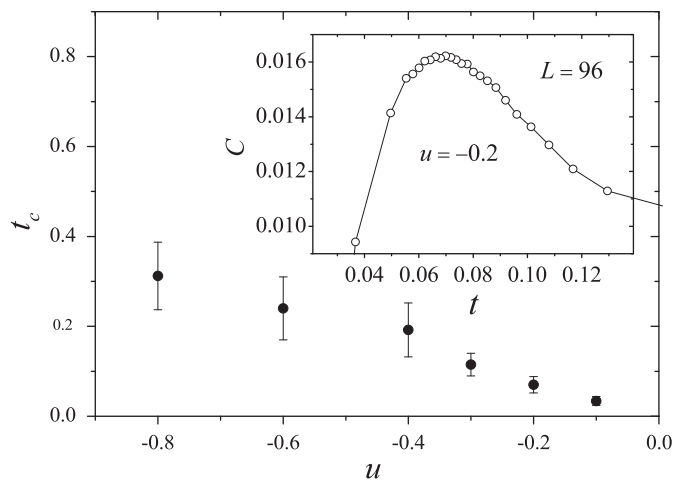

Fig. 11. Same as Figs. 8(a), 9(a), and 10(a) applied to the phase {1/3, 0, 0} found in the energy region $u < 0$. The data were obtained from the location of the heat capacity maximum for $u = -0.2$, as shown in the inset. The error bars correspond to the increasing width of the heat capacity curves.
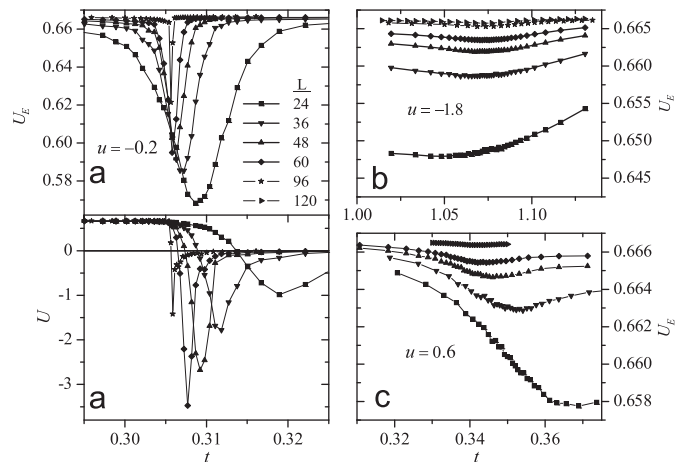
Fig. 12. (a) Energy (U_E) and order parameter (U) cumulant versus temperature t for the {1/2, 0, 1/2} phase; (b) U_E versus t for the {1/2, 1/4, 0} phase; (c) U_E versus t for the {2/3, 1/3, 1} phase. These curves have been generated for sizes $L = 24$, 36, 48, 60, 96, and 120 to determine whether the order-disorder phase transition is first- or second-order.

For the case of {1/2, 0, 1/2}, shown in Fig. 12(a), we find that the U_E- and U-curves suggest the existence of a first-order transition, for both attractive and repulsive second-neighbor interactions. In contrast, the well-studied case $u = 0$ ($W = 0$) of Ref. [24] shows a continuous second-order transition of a new universality class.

The U_E-curves of Figs. 12(b) and (c), corresponding to the phases {1/2, 1/4, 1} and {2/3, 1/3, 1}, respectively, show the characteristics of a second-order transition. The numerical computations in the analysis of the phase {1/3, 0, 0} have been inconclusive and for that reason are not presented.

7. Summary and discussion

The **T**-matrix method has been applied using long double precision arithmetic. It provides the complete study of low temperature dimer adsorption on finite width M square terraces, in the entire range of first- and second-neighbor interactions. With this precision, most of the numerical results are found to fit exact analytic expressions in M. For attractive first-neighbors, we were able to obtain the low-temperature energy phase diagram for any M, thus allowing the straightforward extrapolation to the infinite 2-D surface. For repulsive first-neighbors, the occupational characteristics of the phases all have closed form expressions. We were able to identify phases with increasing values of M which have similar occupational configurations and therefore can be grouped into series in M, which are readily extrapolated to the 2-D surface. However, the low-temperature energy phase diagram in the infinite-M limit could not be uniquely determined based on these results. The definite answer was obtained using MC simulations and finite-size scaling. At low temperature, the long double precision arithmetic has also allowed the study of the transitions between phases, determining whether they are first- or second-order. Since the only phases that survive in the infinite-M limit are those that fit exact analytic expressions in M, the **T**-matrix method also provides, at low temperature, the properties of all of the transitions between the phases of dimers adsorbed on the 2-D surface.

Exchange MC simulations and finite-size scaling have been used in the case of repulsive first-neighbors. They were essential in following the evolution with temperature starting from any of the four ordered phases, identified on the 2-D square surface, reaching the fully disordered state. Some of these transitions have the

signature of second-order transitions, but further work is required to determine the universality class to which they belong and the nature of the remaining transitions. The critical temperature at which these transitions occur depends on the interaction energies, and we provided the complete study of such a relationship.

We have been unable to find experimental data that shows the precise distribution of either bridge sites adsorptions or of two nearest-neighbor monomers' bonds that can therefore be treated as dimers. We would like to suggest experiments capable of determining such a distribution whether on 2-D (1 0 0) surfaces or (1 0 0) terraces of finite width, both at relatively low temperature (to determine the nature of the crystallization patterns) and with increasing temperature (to determine the critical temperature of the transition from the ordered to the disordered state). Comparison between the low temperature results and the low-temperature energy phase diagram of the model (Figs. 5 and 6, or 7) provides a set of constraints on the interaction energies. Comparison between the experimental value obtained for the critical temperature and the curves generated for all possible ordered phases, will further reduce the range of uncertainty on the interaction energies (Figs. 8–11). Low temperature experiments may also be performed to determine the chemical potentials at which transitions between ordered phases occur. It will then become possible to determine the precise interaction energies Eq. (10).

The assumption made above is that the change in pressure or concentration (μ') has a negligible effect on adsorbate–adsorbate interactions (lateral interactions, V and W) or adsorbate–substrate interaction (V_0). For example, consider the low-temperature energy phase diagram associated with the 2-D (1 0 0) surface of Fig. 7, corresponding to repulsive first-neighbors. In this case, no change in the lateral interactions means that u is fixed; and, as μ' is experimentally varied (ν is changing), the evolution of the system is represented in Fig. 7 by a straight-line path parallel to the ν-axis. Then the model predicts six possible sequences of phases with increasing μ' or $\nu = (\mu' + V_0)/|V|$:

1. E→{1/3,0,0}→{1/2,1/4,0}→F, if u is less than -1;
2. E→{1/3,0,0}→{1/2,1/4,0}→{2/3,1/3,1}→F, if u is in the range $(-1, -1/2)$;
3. E→{1/3,0,0}→{1/2,0,1}→{2/3,1/3,1}→F, if u is in the range $(-1/2, 0)$.
4. E→{1/2,0,1}→{2/3,1/3,1}→F, if u is in the range (0, 1).
5. E→{2/3,1/3,1}→F, if u is in the range (1, 2); and
6. a direct transition from empty to full coverage, E→F, if u is greater than 2.

Should the change in pressure or concentration (μ') affect the adsorbate–substrate interaction, V_0, but not the lateral interactions, V and W, this would be experimentally detected from observing a shift between the measured value of ν at the transition between phases and its predicted value, ν_t, given by Eq. (10), since $\nu = (\mu' + V_0)/|V|$.

Finally, should a change in μ' affect the lateral interactions then the path followed in the phase diagram of Fig. 7 will definitely not be parallel to the ν-axis.

Acknowledgements

References

[1] F.Y. Wu, Exactly Solved Models: A Journey in Statistical Mechanics: Selected Papers with Commentaries (1963–2008), World Scientific, 2009.
[2] M. Borowko, W. Rzysko, J. Colloid Interface Sci. 244 (2001) 1.
[3] W. Rzysko, M. Borowko, Thin Solid Films 425 (2003) 304.
[4] W. Rzysko, M. Borowko, J. Chem. Phys. 117 (2002) 4526.
[5] W. Rzysko, M. Borowko, Surf. Sci. 520 (2002) 151.
[6] W. Rzysko, M. Borowko, Surf. Sci. 600 (2006) 890.
[7] W. Rzysko, K. Binder, J. Phys. Condens. Matter 20 (2006) 415101.
[8] G. Rupprechter, T. Dellwig, H. Unterhalt, H.-J. Freund, Topics Catal. 15 (2001) 19.
[9] M. Morkel, G. Rupprechter, H.-J. Freund, J. Chem. Phys. 119 (2003) 10853.
[10] A.J. Phares, F.J. Wunderlich, J.D. Curley, D.W. Grumbine Jr., J. Phys. A Math. Gen. 26 (1993) 6847.
[11] A.J. Phares, D.W. Grumbine, Jr., F.J. Wunderlich, Langmuir 23 (2007) 558.
[12] A.J. Phares, D.W. Grumbine, Jr., F.J. Wunderlich, Langmuir 26 (2010) 10750.
[13] A.J. Phares, D.W. Grumbine, Jr., F.J. Wunderlich, Langmuir 25 (2009) 13467.
[14] A.J. Phares, D.W. Grumbine, Jr., F.J. Wunderlich, Langmuir 25 (2009) 944.
[15] A.J. Phares, D.W. Grumbine, Jr., F.J. Wunderlich, Langmuir 24 (2008) 11722.
[16] A.J. Phares, D.W. Grumbine, Jr., F.J. Wunderlich, Langmuir 24 (2008) 124.
[17] A.J. Phares, D.W. Grumbine, Jr., F.J. Wunderlich, Phys. Lett. A 366 (2007) 497.
[18] A.J. Phares, D.W. Grumbine, Jr., F.J. Wunderlich, Langmuir 23 (2007) 1928.
[19] A.J. Phares, D.W. Grumbine, Jr., F.J. Wunderlich, Langmuir 22 (2006) 7646.
[20] P.W. Kasteleyn, Physica 27 (1961) 1209.
[21] K. Hukushima, K. Nemoto, J. Phys. Soc. Jpn. 65 (1996) 1604.
[22] D.J. Earl, M.W. Deem, Phys. Chem. Chem. Phys. 7 (2005) 3910.
[23] N. Metropolis, A.W. Rosenbluth, M.N. Rosenbluth, A.H. Teller, E. Teller, J. Chem. Phys. 21 (1953) 1087.
[24] F. Romá, A.J. Ramirez-Pastor, J.L. Riccardo, Phys. Rev. B 72 (2005) 035444.
[25] F. Romá, A.J. Ramirez-Pastor, J.L. Riccardo, Phys. Rev. B 77 (2008) 195401.
[26] K. Binder, Applications of the Monte Carlo Method in Statistical Physics: Topics in Current Physics, vol. 36, Springer, Berlin, 1984.
[27] F. Romá, A.J. Ramirez-Pastor, J.L. Riccardo, Langmuir 19 (2003) 6770.
[28] M.S.S. Challa, D.P. Landau, K. Binder, Phys. Rev. B 34 (1986) 1841.
[29] A. Billoire, R. Lacaze, A. Morel, S. Gupta, A. Irbäck, B. Petersson, Phys. Rev. B 42 (1990) 6743.
[30] K. Vollmayr, J.D. Reger, M. Scheucher, K.Z. Binder, Phys. B 91 (1993) 113.
[31] E. Rastelli, S. Regina, A. Tassi, Phys. Rev. B 71 (2005) 174406.